Review

Cell PRESS

Photoacoustic imaging in cancer detection, diagnosis, and treatment guidance

Srivalleesha Mallidi, Geoffrey P. Luke and Stanislav Emelianov

Department of Biomedical Engineering, University of Texas at Austin, Austin, TX 78712, USA

Imaging modalities play an important role in the clinical management of cancer, including screening, diagnosis, treatment planning and therapy monitoring. Owing to increased research efforts during the past two decades, photoacoustic imaging (a non-ionizing, noninvasive technique capable of visualizing optical absorption properties of tissue at reasonable depth, with the spatial resolution of ultrasound) has emerged. Ultrasound-guided photoacoustics is noted for its ability to provide *in vivo* morphological and functional information about the tumor within the surrounding tissue. With the recent advent of targeted contrast agents, photoacoustics is now also capable of *in vivo* molecular imaging, thus facilitating further molecular and cellular characterization of cancer. This review examines the role of photoacoustics and photoacoustic-augmented imaging techniques in comprehensive cancer detection, diagnosis and treatment guidance.

Introduction

Cancer is a vicious disease that killed approximately 570 000 people in 2010 in the USA alone [1]. To develop successful therapeutic strategies and prevent recurrence of the disease, its structural, functional and metabolic properties need to be well characterized. Research efforts are focused not only on developing new treatments and discovering the root cause for the disease, but also on developing imaging technologies that can aid in early detection of cancer and can provide comprehensive real-time information on the tumor properties. Currently, ultrasound imaging (USI), magnetic resonance imaging (MRI), X-ray computed tomography (CT) and nuclear imaging techniques, such as positron emission tomography (PET) and single photon emission computed tomography (SPECT), are being used to detect tumors in patients [2]. With the development of various targeted contrast agents, these imaging techniques are also able to provide molecular information about the malignant tumor tissue. However, microscopic optical imaging techniques have higher resolution (~0.1–100 μm) compared with USI (50–500 μm), MRI (10–100 μm), CT (50–200 μm), PET (1–2 mm) and SPECT (1–2 mm), and can detect a lower number of cancer cells per imaging voxel [3]. Traditional diffusive regime optical imaging techniques, such as diffuse optical tomography (DOT), have high detection sensitivity; however, their resolution is limited to approximately 5 mm. The need for an imaging technique that can provide high optical contrast images at a microscale resolution and at a reasonable penetration depth has now been filled by photoacoustic imaging (PAI).

PAI has shown tremendous potential in simultaneously providing structural, functional and molecular information in preclinical studies. PAI can visualize tumor location deep within a tissue, and is also able to provide information on tumor vasculature [4] or to monitor angiogenesis [5]. PAI can also obtain information on hemoglobin oxygen saturation at high resolution and contrast, without the use of exogenous contrast agents [4], which is a significant advantage when compared with other tumor hypoxia imaging techniques (e.g., blood oxygen level-dependent MRI and PET). Another advantage of PAI is its compatibility with widely available USI techniques [6]; when combined, PAI and USI can simultaneously provide anatomical and functional information on tumors. For example, an *in vivo* study on human breast tissue has shown that an ultrasound image can depict the structure of ductal carcinoma, whereas photoacoustic (PA) images show the associated scattered distribution of vascularization [7].

With the availability of various targeted contrast agents, such as gold nanoparticles (AuNPs), several new avenues have opened for *in vivo* molecular PAI. This has facilitated highly sensitive and specific detection of tumors. In addition, PAI, combined with other complementary imaging techniques, has shown promise in cancer treatment guidance. Although several reviews on the basics and applications of PAI have been published, no examination of the recent developments in molecular PAI of cancer and the ability of PAI to monitor treatment is currently available; hence, we review these topics here.

Basic principles of PAI

PAI (also known as optoacoustic imaging) capitalizes on the PA effect first described by Alexander Graham Bell in 1880 [8]. In this review, we provide only basic principles (Box 1) towards understanding PAI applicability to cancer detection and treatment guidance. Briefly, absorbed laser energy causes a rapid thermoelastic expansion of tissue, resulting in the generation of a wide-band ultrasound wave. The ultrasound wave is detected with a transducer

Corresponding author: Emelianov, S. (emelian@mail.utexas.edu).

0167-7799/$ – see front matter doi:10.1016/j.tibtech.2011.01.006 Trends in Biotechnology, May 2011, Vol. 29, No. 5

Box 1. Principles of PAI

To describe the PA effect, a simplified Equation I, assuming 1D plane-wave propagation in a homogeneous medium, can be used:

$$p_0 = \frac{\beta v_s^2}{C_p}\mu_a F_0 e^{-\mu_{eff} z} = \Gamma \mu_a F_0 e^{-\mu_{eff} z} \quad \text{(I)}$$

where p_0 is the pressure rise immediately after thermoacoustic excitation in the photoabsorber; β is the thermal coefficient of volume expansion; v_s is the speed of sound in tissue; C_p is the specific heat capacity of the tissue at constant pressure; μ_a represents the optical absorption coefficient of the photoabsorber; F_0 is the laser fluence at depth $z = 0$; Γ is the Gruneisen parameter or coefficient; and μ_{eff} is the effective extinction coefficient of the tissue, defined in Equation II as:

$$\mu_{eff} = \sqrt{3\mu_a(\mu_a + \mu_s')} \quad \text{(II)}$$

where μ_s is the scattering coefficient of tissue [6,9,10,65]. In practice, optical heterogeneities of the tissue and other effects can significantly complicate Equation I.

PAI spatial resolution is determined by the overlap of optical and ultrasound beams [6,11,66]. For deep-penetrating PAI, the parameters of the ultrasound transducer are the most crucial: the axial resolution is inversely proportional to the transducer bandwidth (BW), and the lateral resolution is inversely proportional to the numerical aperture (NA) and center frequency of the transducer. Therefore, a transducer with high center frequency, high bandwidth and large NA yields the best resolution images [6,11].

Penetration depth in PAI is limited by the wavelength of laser illumination. Greater penetration depth can be achieved in the optical window (600–1100 nm) where tissue endogenous chromophores have less optical absorption. Imaging depths of up to 5–6 cm have been achieved [47,67,68] using radiant exposures below the maximum permissible exposure (MPE) imposed by the American National Standards Institute for human skin. The MPE limit at different wavelengths is 20 mJ/cm^2 at $400<\lambda<700$ nm; $20 \times 10^{0.002(\lambda-700)}$ mJ/cm^2 at $700<\lambda<1050$ nm; and 100 mJ/cm^2 at $1050<\lambda<1500$ nm [69].

There is a trade-off between imaging depth and resolution of PAI. As the imaging depth increases, frequency-dependent attenuation decreases the BW and center frequency of the ultrasound wave, resulting in poorer spatial resolution (Table I) [6]. Thus, several PAI systems have been developed to image both microscopic and macroscopic features of tumors [9]. PA microscopy systems sacrifice imaging depth to improve resolution to as low as 50 μm [4,6,70,71]. With a highly focused laser beam, a lateral resolution of 5 μm can be reached to image superficial capillaries [70]. Conversely, macroscopic PAI systems, with resolution on the order of hundreds of microns, are promising for tumor detection in deeper regions [15,47,67,68].

Table I. Common USI and PAI imaging parameters

Parameter	Transducer frequency (MHz)	Axial resolution (μm)	Lateral resolution (μm)	Imaging depth (mm)
Ultrasound	5	150	300	70
	20	75	165	30
Macroscopic PAI	5	150	300	40
Microscopic PAI	50	15	50	3
Optical resolution PAI	75	15	5	0.7

that converts the mechanical acoustic waves to electric signals. The captured signals are then processed to form an image [6,9,10]. A typical PAI setup (Figure 1a) consists of two main components: a laser (generally a tunable, nanosecond pulsed laser) and a USI system. Most ultrasound image processing techniques translate directly to PAI. Delay and sum beamforming or more advanced computed tomography algorithms used in USI are also used in PAI to obtain images [10,11]. Other reviews have provided detailed information on equations governing the PA effect, various PA system configurations and the image processing algorithms [6,9–12].

The contrast in PA images is largely determined by the wavelength-dependent μ_a (Equation I, Box 1). The changes in optical absorption as a function of wavelength for a variety of endogenous chromophores, including melanin, oxy- (HbO_2) and deoxyhemoglobin (Hb) are presented in Figure 1b. Because of the large variations in μ_a, spectroscopic or multi-wavelength imaging techniques are used for characterization of tumor tissue optical properties. For example, HbO_2 and Hb have different wavelength-dependent optical absorption properties, which enables spectroscopic PAI to differentiate between arteries and veins. Furthermore, HbO_2 and Hb have the same optical absorption at approximately 805 nm; PAI at this and other wavelengths can be used to assess total hemoglobin and blood oxygenation. PA contrast can also be enhanced by exogenous contrast agents (e.g., dyes or nanoparticles; Figure 1c) that have distinct and tunable absorption spectra in the near-infrared (NIR) optical window (600–1100 nm) where endogenous chromophores, such as hemoglobin and water, have low absorption (Figure 1b).

Cancer detection with endogenous PA contrast

Cancer detection using PAI with endogenous chromophores (e.g., hemoglobin and melanin) is an area of active research. For example, PAI has been used to monitor melanoma tumor growth over the course of two weeks [13]. Optical contrast was provided by a higher concentration of melanin in the tumor relative to the surrounding tissue. PAI has also been used to detect skin melanoma [4,14]. Figure 2a depicts a melanoma and surrounding vasculature obtained by spectroscopic PAI. The pseudo-colored image was reconstructed from PA images obtained at 584 nm and 764 nm laser illumination. These studies indicate that PAI has the potential to identify, visualize and track tumors and their associated vasculature with high resolution.

Malignant tumors have dense and unorganized vasculature compared with normal tissue. The high density of blood vessels in tumors enhances PA image contrast, thereby enabling tumor detection. For example, the Twente Photoacoustic Mammoscope, developed to detect breast carcinoma, was based on this principle [15,16]. In Figure 2, an X-ray mammogram (Figure 2b-i) and a sonogram (Figure 2b-ii) are compared with a PA image (Figure 2b-iii) obtained with a 1064 nm optical source. Figure 2 shows that the mammoscope is more sensitive to malignant indicators, such as vascularization, than are conventional radiological techniques. PAI can also provide

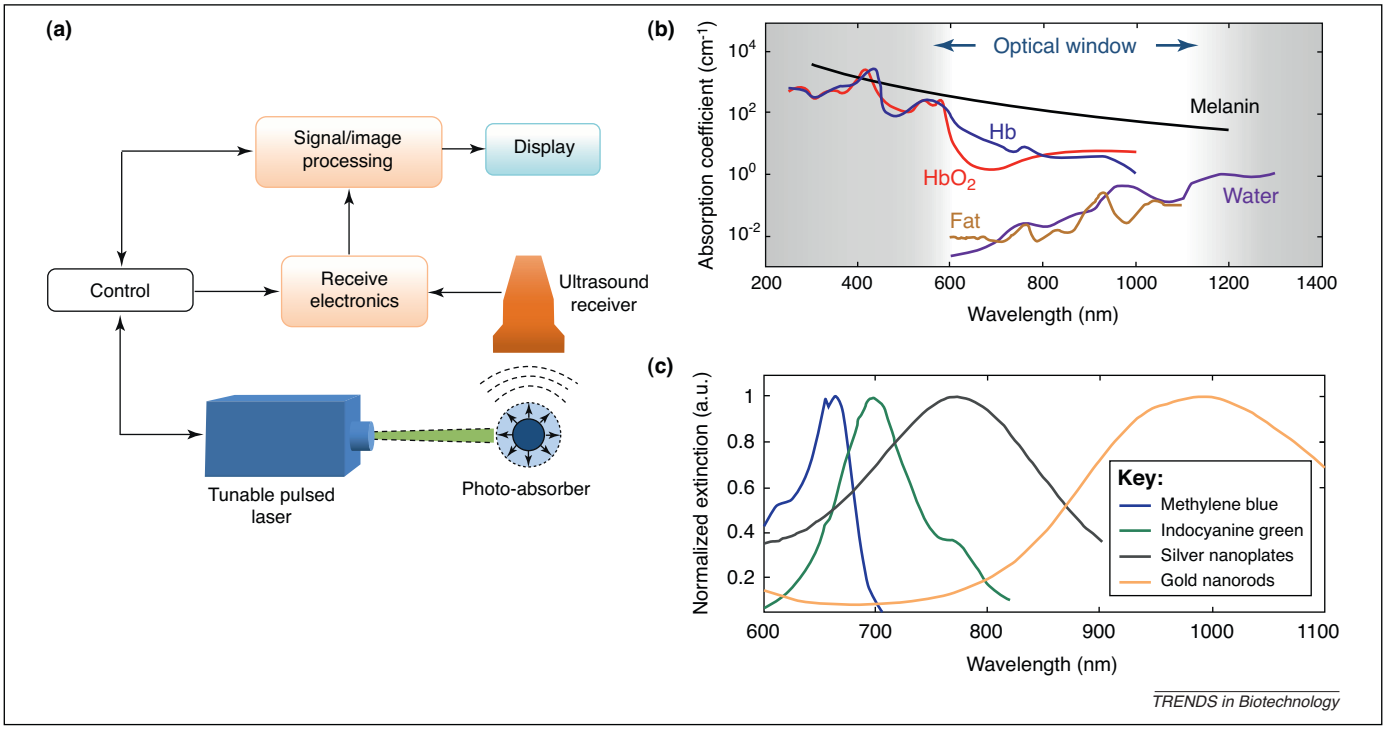

Figure 1. PAI principles **(a)** Block diagram of a typical PAI system. **(b)** Absorption spectra of endogenous chromophores in the body. The optical absorption of these endogenous chromophores is wavelength dependent; therefore, the PA signal intensity at different optical wavelengths can be used to characterize optical properties of tissue. Data for the absorption coefficient were obtained from http://omlc.ogi.edu/spectra/. The 'optical window' (600–1100 nm) is the wavelength range in which tissue absorption is at a minimum. **(c)** Extinction spectra of common exogenous contrast agents with peaks in the optical window.

information on angiogenesis or changes in vasculature [5,17–19]. As shown in Figure 2c, sequential PA images can be obtained safely and noninvasively at different stages of tumor progression to monitor angiogenesis and to determine whether a tumor has progressed to malignancy [5]. Compared with other vascular imaging techniques, including dynamic-enhanced MRI, CT perfusion and functional PET [20], PAI detects tumor vasculature at a better or comparable resolution, without the use of exogenous contrast agents.

Besides imaging melanin and blood vessels, PAI systems have been used for measuring the oxygen content of blood to study hypoxia in tumors [21,22]. Hypoxia is often linked to malignancy and resistance to therapy [23]. The amount of oxygen saturation in blood (SO_2) can be estimated by comparing the PA signal strength of HbO_2 and Hb obtained from spectroscopic PA images. Figure 2d shows *in vivo* functional imaging of a mouse brain with a glioblastoma. The blue hypoxic region (circled) indicates the location of the tumor in the brain [22]. The results clearly depict that the tumor has a lower percentage SO_2 than the surrounding normal tissue.

Metastatic spread of the primary tumor often leads to death in patients with cancer. Highly sensitive detection of circulating tumor cells (CTCs) would greatly enhance overall patient survival, if treated. PAI has been used to detect CTCs in the blood stream, with the goal of detecting metastasis. The label-free detection of CTCs *in vivo* in a blood vessel using PAI could provide higher detection sensitivity (~100-fold) compared with existing *ex vivo* CTC detection assays that use a small amount of blood. With the use of contrast agents targeted to CTCs, the PAI detection sensitivity can be enhanced further [24–26].

Cancer detection with exogenous PA contrast agents

The sensitivity of the PAI technique to image deeply situated tumors can be increased dramatically by utilizing exogenous contrast agents. The NIR-absorbing dyes, such as IRDye800CW [22,27], AlexaFluor 750 [28] and indocyanine green (ICG) [29], have been used to enhance PA contrast. However, among the exogenous contrast agents, AuNPs have attracted attention in nanoparticle-based PAI owing to their unique optical properties from the surface plasmon resonance (SPR) effect. Because of the SPR effect, AuNPs have an absorbance that is orders of magnitude higher than that of NIR dyes. For example, gold nanospheres, nanorods, nanoshells, nanocages and nanobeacons have been used in PAI because of their tunable and strong longitudinal plasmon resonance in the NIR [30–37]. The cytotoxicity of these nanoparticles is debatable and often emerges in a dose- and time-dependent manner for different types of nanoparticle; hence, further investigation into the toxicity of AuNPs is necessary [38]. The details on toxicity and pharmacodynamics of nanoparticles are beyond the scope of this review and are therefore not discussed here.

By attaching targeting moieties to exogenous agents, specific molecular information regarding tumors can be obtained. AuNPs with different optical absorption properties can be conjugated to cancer-specific biomarkers, such as growth factor receptors and integrins (Table 1). By utilizing multiple targeted AuNPs, multiplex molecular labeling of a tumor can be achieved and multi-wavelength PAI can image the heterogeneous accumulation and interaction of AuNPs with cancer cells *in vivo* [32]. Fluorescent optical probes, such as quantum dots, also provide PA contrast and can be used for multiplex labeling of tumors [39].

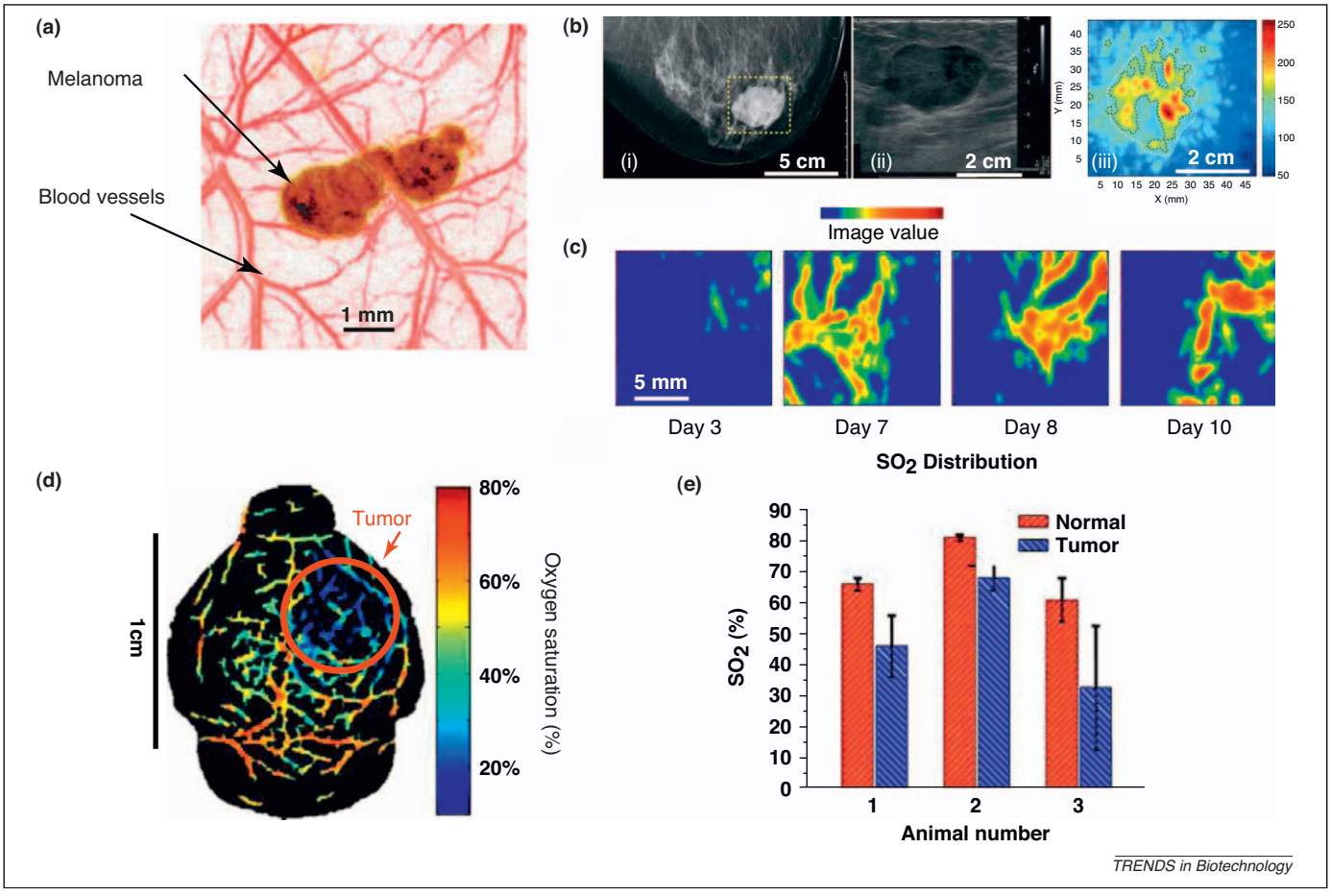

Figure 2. PAI of tumors using endogenous contrast **(a)** Overlaid maximum amplitude projections of PA images at 764 nm and 584 nm showing a tumor and its surrounding vasculature, respectively. The image clearly shows the vessel branching and structure around the tumor. **(b)** Images of the breast of a 57-year-old woman with invasive ductal carcinoma: **(i)** X-ray mammogram; **(ii)** sonogram; and **(iii)** PA image at 1064 nm. The X-ray mammogram and the sonogram depict the gross anatomical features of the tumor, but do not provide functional information. The high PA amplitude corresponds with abundant vasculature associated with malignant tumors. The PA image clearly depicts higher vascular densities in the tumor periphery, whereas the core of the tumor has minimum vasculature. **(c)** Pancreatic tumor cells were inoculated on a rat hind leg on day 1. PAI was used to monitor angiogenesis associated with the tumor growth.PA images obtained from the tumor region on days 3, 7, 8 and 10 are maximum intensity projections of the PA source strength in the xy-plane (i.e., top view on the tumor tissue). **(d)** *In vivo* functional imaging of a mouse brain with a glioblastoma xenograft obtained using PAI. Spectroscopic PAI (wavelengths from 764 nm to 824 nm) was used to detect hypoxia in a brain tumor. The heat map represents the percentage SO_2 in the blood vessels (blue = hypoxic; red = hyperoxic). The area indicated by the red arrow is the tumor. **(e)** A comparison of normal (red bars) and brain tumor (blue bars) vasculature SO_2in three mice. Three normal vessels and three tumor vessels were chosen from each SO_2 image that had been processed from spectroscopic PA images, such as the one shown in **(d)**. The results clearly indicate that the percentage SO_2 in tumors is lower than in the surrounding normal tissue, thus indicating hypoxia. Adapted with permission from [4] **(a)**, [15] **(b)**, [5] **(c)** and [22] **(d,e)**.

Table 1. Exogenous PA contrast agents used for detecting tumors *in vivo*

Contrast agent	λ_{peak} (nm)[b]	Tumor type	Target	Refs
IRDye800[a]	800	Glioblastoma	Integrin $\alpha_v\beta_3$	[22]
IRDye800	800	Breast cancer	Neutropilin-1 receptor	[27]
Gold nanocages	778	Melanoma	Melanocyte-stimulating hormone	[30]
Gold nanorods	785 or 1000	Squamous cell carcinoma	HER2[d] and EGFR	[32]
Gold nanorods	810	Prostate cancer	HER2	[33]
Gold nanoshells	800	Colon carcinoma	None	[34]
Gold nanospheres	525	Breast cancer	None	[36]
Green-dye-enhanced single-walled carbon nanotube (SWNT-ICG)	780	Glioblastoma	Integrin $\alpha_v\beta_3$	[72]
Silver nanoplates	1064	Pancreatic cancer	None	[73]
SWNT	750[c]	Glioblastoma	Integrin $\alpha_v\beta_3$	[74]
SWNT	690[c]	Glioblastoma	Integrin $\alpha_v\beta_3$	[75]

[a]IRDye800 (Li-Cor) was conjugated with a cyclic peptide that targets integrin $\alpha_v\beta_3$.

[b]λ_{peak} indicates the optical absorption peak of the nanoparticles and the wavelength at which PAI was performed.

[c]Nanoparticles such as carbon nanotubes do not have distinct optical absorption peaks in the optical window. For such nanoparticles, an optimum wavelength is chosen by the researchers to obtain a PA image with enhanced contrast. In the table, the wavelength at which PAI was performed is considered the 'imaging' rather than the 'peak'λ.

[d]Abbreviation: HER2, human epidermal growth factor receptor 2.

There have been several advances in molecular PAI that help describe crucial functional and molecular interactions between tumor cells and the surrounding microenvironment. For example, the feasibility of utilizing a multi-wavelength PAI technique to monitor molecular interactions of epithelial growth factor receptor (EGFR)-targeted AuNPs in 3D tissue cultures and *ex vivo* tissue has been evaluated [35,40]. Briefly, AuNPs (spheres of 50 nm diameter) functionalized with antibodies bind to EGFR. This specific targeting of AuNPs to EGFR causes plasmon resonance coupling between adjacent nanoparticles and changes their absorbance spectra so that it can be detected as a change in the PA signal amplitude. Overall, the results indicate that PAI together with bioconjugated AuNPs have the potential to image nanomolecular interactions. Because of the concerns that nanoscale agents might cause long-term toxicity *in vivo*, biodegradable gold nanoclusters have been developed as a contrast agent [41,42]. The size of these biodegradable nanoclusters, consisting of sub-5-nm AuNPs and a biodegradable polymer binder, is less than 100 nm. The nanoclusters are also pH sensitive and will biodegrade in the acidic environment of the endosome. After degradation, the 5-nm AuNPs are excreted out of the body, thereby preventing toxic accumulations.

Another recent advancement in PAI is the use of photoactivable probes to provide a target-dependent PA signal; they show superior specificity and sensitivity compared with the probes that do not interact with the target. For example, photoactivable probes have been designed to target matrix metalloprotease 2 (MMP-2) specifically, a protease found to be overexpressed in many aggressive cancers [43]. The peptide platform of the probe consists of an activatable cell-penetrating peptide (ACPP) that is recognizable by MMP-2 in both *in vitro* and mouse models. Before cleavage by MMP-2, the intact probe shows PA signals of similar intensity at the two wavelengths corresponding with the absorption maxima of the chromophores BHQ3 (675 nm) and AlexaFluor 750 (750 nm). When the probe is cleaved by the appropriate enzyme, the BHQ3 dye associated with the CPP portion of the probe accumulates in the nearby cells, whereas the Alexa dye diffuses away. This results in a PA signal visible only at 675 nm [43].

Recently, emphasis has been placed on multimodal nanosystems that can enhance contrast in two or more imaging modalities, including microbubbles [44], perfluorocarbon-based nanobubbles [45] and nanowontons [46]. For example, nanowontons consist of a ferromagnetic (cobalt core) core coated with gold for biocompatibility and a unique shape that enables optical absorption over a broad range of frequencies; the magnetic core acts as an MRI contrast agent and the gold coating provides the optical absorption contrast for PAI [46]. With the evolution of combined imaging strategies, these multimodal nanostructures will play a prominent role in cancer detection and treatment.

Combination of PA with other imaging modalities

Assessing complementary structural, functional, metabolic and molecular information on a tumor with high accuracy is essential for cancer treatment. PAI primarily provides high-resolution images based on the optical contrast of tissue components, such as changes owing to abnormal vasculature or high melanin content; however, the overall anatomical structure of the tumor cannot be perceived by PAI alone. USI, a noninvasive technique, can be used to obtain anatomical details about the tumor and its surrounding environment (Figure 3a). Both USI and PAI are highly synergistic: they utilize the same transducer and receiver electronics and are non-ionizing imaging modalities (unlike CT and PET) [6]. Indeed, commercial ultrasound systems have been modified to PAI systems for both small animal imaging and breast cancer imaging [7,12,47–50].

An imaging modality that can provide structural information at resolutions greater than ultrasound (~50–500 μm) is optical coherence tomography (OCT; ~10 μm), which relies on the optical backscattering properties of tissue. A 3D combined OCT and PA system has been constructed that can image microvasculature circulation (Figure 3b) [51]. This combined system could be used to image the microvasculature of malignant skin lesions and provide comprehensive structural and functional information [52]. Other optical imaging modalities, such as fluorescence (FL) imaging (Figure 3c), have also been used with PAI to image brain tumors *in vivo* [22]. PAI provides high-resolution structural images of tumor angiogenesis, whereas FL imaging has high sensitivity to molecular probes for detecting tumor location.

Ultrasound-based elasticity imaging noninvasively assesses the biomechanical properties (i.e., the Young's modulus) of tumors, which otherwise cannot be depicted from ultrasound or PA images (Figure 3d). A combination of ultrasound and elasticity imaging has shown the best results in detecting breast tumors *in vivo* with high sensitivity and specificity, and could reduce the number of unnecessary biopsies [53]. A combination of complementary imaging techniques (e.g. elasticity coupled with USI and PAI) could further improve cancer detection sensitivity and specificity by providing simultaneous information on anatomy (USI), angiogenesis (PAI) and changes in mechanical properties (elasticity imaging) of the tumor [6]. Another ultrasound-based imaging technique that can be combined with PAI is magneto-motive USI (MMUS). MMUS has the potential to measure the biomechanical properties of the tissue with the aid of magnetic nanoparticles (Figure 3e) [54]. In MMUS, magnetic excitation is applied to induce motion of the magnetic nanoparticles within tissues or organs. The mechanical properties of the tissue can be evaluated based on tissue motion detected in ultrasound images [55]. Based on the initial studies performed on tissue-mimicking phantoms, it can be predicted that the pathological changes in tissue, which are often related to changes in tissue mechanical properties, could be detected and differentiated using MMUS. However, further investigation in murine tumor models is required to evaluate the technique *in vivo*. With the recent introduction of *in vivo* imaging systems (e.g., Vevo 2100 by Visual Sonics Inc.) capable of both USI and PAI at microscopic or macroscopic resolution, the functional intricacies and the structural complexities of the tumor can be visualized simultaneously.

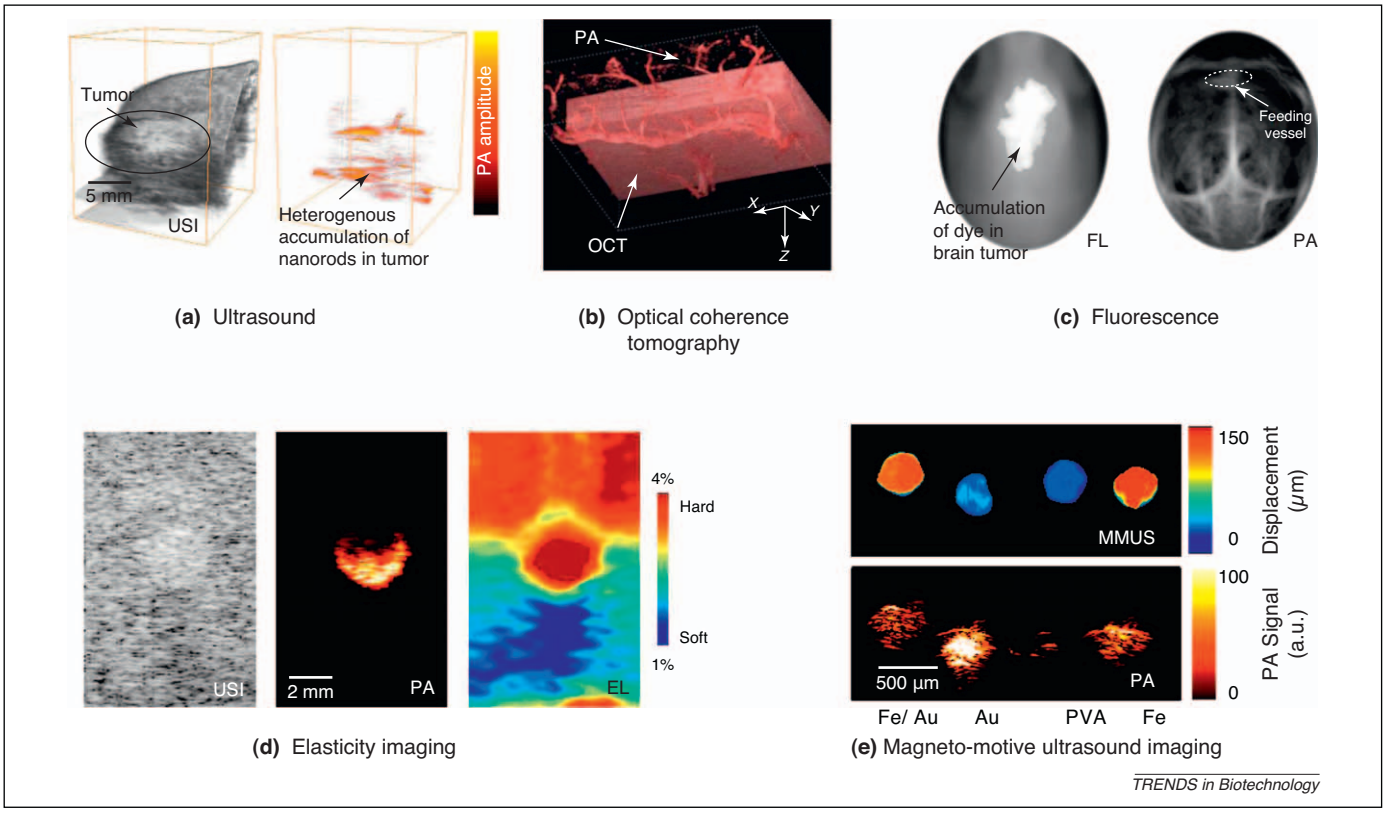

Figure 3. Various optical- and ultrasound-based imaging techniques can be combined with PAI to provide structural, functional and biomechanical properties of the tissue. **(a)** *In vivo* 3D USI and PAI of a subcutaneous tumor in a mouse injected with gold nanorods. The subcutaneous tumor appears as a bump in the 3D ultrasound image. The PA image shows the heterogeneous localization of nanorods in the tumor, which accumulate there preferentially owing to the enhanced permeation and retention effect [76]. **(b)** *In vivo* PAI and OCT of the skin on the back of a nude mouse. The image represents a data fusion of OCT (structure of the skin) and PA (microvasculature) images. **(c)** Noninvasive *in vivo* FL image acquired 24 hours after ICG injection in a mouse with melanoma cells implanted in its brain. Noninvasive *in vivo* PA images were acquired with the skin and skull intact, showing the vasculature in the brain. **(d)** Gray-scale ultrasound image **(i)**, PA image **(ii)**, and elasticity **(iii)** images of a tissue-mimicking phantom with a single inclusion. The inclusion had higher optical contrast and was harder compared with the background. **(e)** MMUS **(i)** and PA **(ii)** images of a tissue-mimicking phantom with samples containing (left to right): a mixture of Fe_3O_4 nanoparticles and AuNS; AuNS only; PVA only (no nanoparticles); and Fe_3O_4 nanoparticles only. The MMUS color map represents the displacement of the inclusions. The pure PVA sample (no nanoparticles) did not displace under magnetic excitation and showed no PA contrast. The AuNS also did not displace, but had high optical absorption and hence produced greater PA signals compared with Fe_3O_4 nanoparticles. The two samples containing Fe_3O_4 nanoparticles had a displacement of approximately 100 μm [78]. Adapted, with permission, from [51] (b) and [77] (c).

PAI for guiding, monitoring and evaluating therapy

Imaging techniques play a significant role in cancer therapy, from precise planning and guiding to evaluation of efficacy. In particular, PAI has shown potential in aiding therapies by providing sequential monitoring of tumor functional properties, such as changes in tumor vasculature before, during and after therapeutic procedures. The therapeutic agents used for photodynamic therapy (PDT) or photothermal therapy (PTT) can also act as PA contrast agents, owing to their high optical absorption properties in the NIR region (e.g., protoporphyrin IX for PDT and gold nanorods for PTT) [32,56].

PAI can assist in determining the location of the tumor, gauging the heterogeneities in vasculature within it and observing the heterogeneities in the therapeutic agent accumulation. For example, golden carbon nanotubes (GNTs) conjugated with an antibody specific to the lymphatic endothelial hyaluronan receptor-1 have been used to visualize heterogeneities of endogenous low-absorbing mesenteric structures in a nude mouse (Figure 4a) [57]. The PA image provided information on the heterogeneous accumulation of targeted GNTs (red regions in Figure 4a) to guide PTT to cause spatially specific thermal damage to the lymphatic walls [57]. In another study, PAI was performed to identify the location of a colon adenocarcinoma tumor. The tumor was then specifically ablated by high-intensity focused ultrasound (HIFU) with the guidance of PA images [58].

PAI has tremendous potential in guiding therapeutic procedures and could provide oncologists with structural and functional information regarding tumors to facilitate personalized therapy by customizing the therapy dose. In addition, PAI can also aid in the customized delivery of drugs with use of multifunctional nanoparticles. An example of such a nanoagent is a silver nanosystem consisting of a poly(lactic-*co*-glycolic acid) (PLGA) polymer core and outer silver cage network. The outer silver cage enhances contrast in PAI and the inner core of the nanosystem contains the drug doxorubicin (Figure 4b). Initial studies indicated that the PLGA-based nanosystems have the potential to increase contrast significantly in PAI while delivering customized payloads of drug simultaneously to the tumor cells [59]. Another example of controlled and customized drug delivery is using light-triggered nanoconstructs, such as microspheres containing the drug paclitaxel encapsulated in hollow gold nanospheres (HAuNS). Depending on the concentration of HAuNS in the tumor, the light dose can be adjusted to allow sufficient release of paclitaxel [60]. In addition, HAuNS can also act as a PTT agent. Few *in vitro* studies are published illustrating these

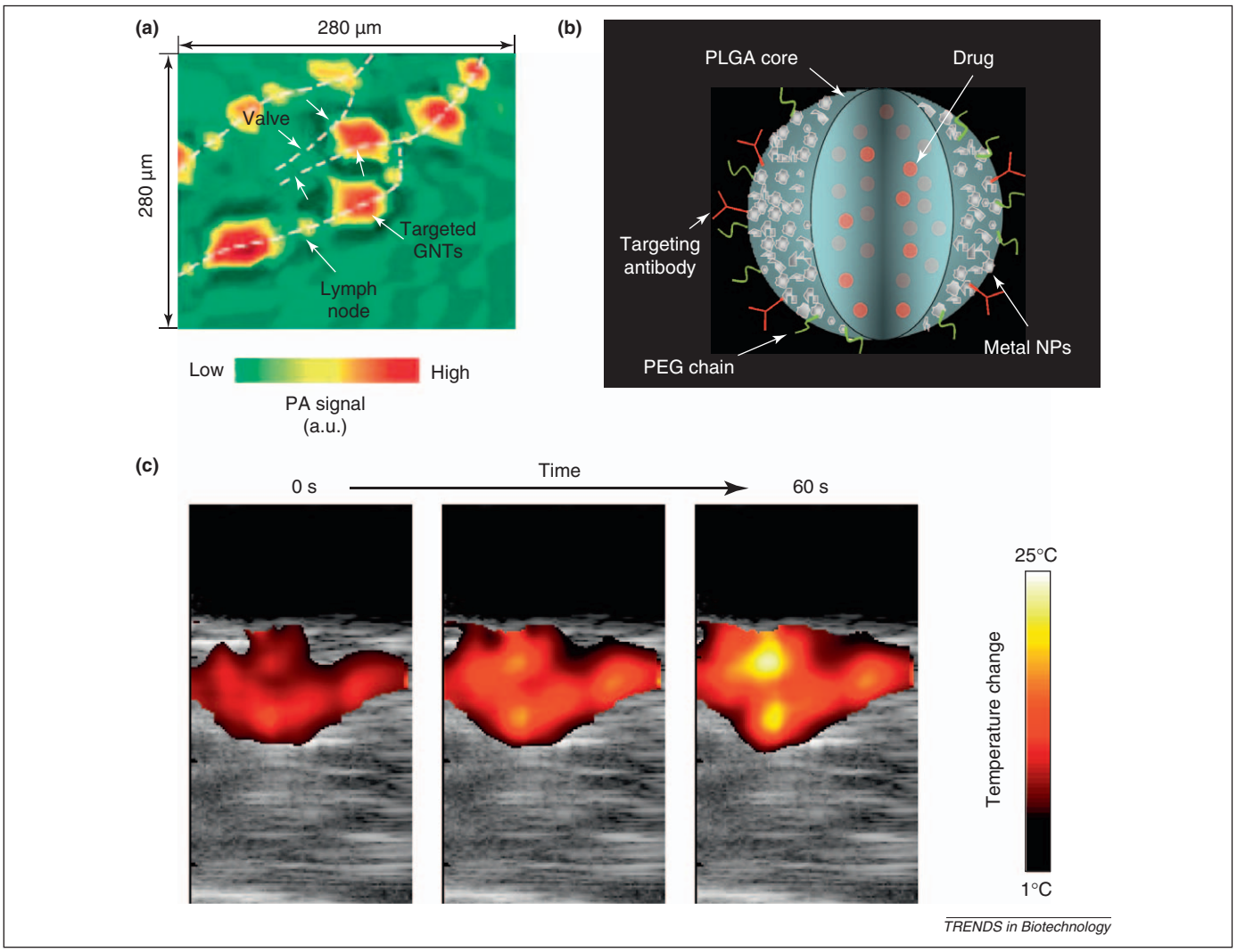

Figure 4. PAI for guiding and monitoring therapy **(a)** PAI can guide therapeutic procedures by providing an accurate biodistribution map of therapy agents. The white dashed lines represent the lymph node. The red regions indicate areas of higher accumulation of GNTs (i.e., in the lymph nodes). Therapeutic localization and dosage can be decided based on the guidance provided by the PA image regarding the location of GNTs. **(b)** Doxorubicin is encapsulated in the PLGA core, and the silver metal nanoparticles on the surface provide PA contrast for monitoring therapeutic response. **(c)** Therapeutic efficacy can be monitored in the context of the anatomical map of the tumor tissue. USI and PAI can be used to monitor the temperature increase during thermal therapy procedures. A mouse was injected with optically absorbing gold nanorods that acted as both PA and photothermal agents. The tumor region was then irradiated with continuous-wave laser light at the peak absorption wavelength. Images taken after 0, 30 and 60 seconds of treatment indicated that the relative temperature rise in the tumor was 25 °C. Each image represents a 10.5 mm × 20 mm field of view. Adapted, with permission, from [57] **(a)** and [59] **(b)**.

concepts and further investigations of *in vivo* tumor models are required for validation.

Monitoring functional or structural changes, such as changes in tumor tissue properties and variations in vascular destruction during therapeutic procedures, is crucial for prognosis and further treatment. Several *ex vivo* studies show the potential of PAI in monitoring therapeutic procedures. For example, it has been demonstrated using *ex vivo* liver tissue and chicken breast tissue that PAI is capable of sensitive detection of thermally induced changes in tissue optical properties at depths of up to 30–50 mm with submillimeter resolution during thermal therapy [61,62]. In another study, PAI provided both high-resolution and high-tissue-contrast images to quantify changes in vessel morphology during PDT using protoporphyrin IX photosensitizer on a chicken chorioallantoic membrane tumor model [56].

In PTT, efficient optical absorbers, such as gold nanorods, are used to heat the tissue to higher temperatures, causing thermal damage. For example, a tumor loaded with gold nanorods showed significant temperature elevations in response to laser irradiation (Figure 4c). Both PAI and USI can be used to obtain temperature maps of the tumor during PTT. Indeed, PA-based thermal imaging in the presence of strong optical absorbers has a higher signal:noise ratio when compared with USI-based thermal imaging [63]. The examples provided in this section clearly indicate the potential of PAI for guiding, customizing and monitoring therapeutic procedures.

Outlook

Overall, PAI could become a valuable tool for cancer detection and diagnosis, tumor characterization and treatment guidance. By differentiating the optical properties of tissues, PAI is well suited to measuring the functional properties of tumors *in vivo*. For example, multi-wavelength PAI can visualize vasculature and identify hypoxic conditions within a tumor. Current functional imaging techniques suffer from

either poor spatial resolution or inadequate penetration depth. Conversely, PAI is non-ionizing and can image deep tissue structures with acceptable spatial resolution.

For functional cellular and molecular imaging *in vivo* at sufficient depths, contrast agent-mediated PA holds great promise. Various PA contrast agents, ranging from plasmonic metal nanoparticles to FDA-approved dyes, can be targeted to specific receptors in intact living tissue. Compared with endogenous contrast of tissue, PA contrast agents can be tuned to a specific wavelength to provide images with higher contrast and signal-to-noise ratio. As with any exogenous contrast agent, the safety and biocompatibility of the agents must be further addressed.

PAI might also play an important role in several existing and emerging treatment modalities. It can image metal objects (e.g., needles, brachytherapy seeds and stents) and, therefore, guide therapeutic interventions [64]. The temperature dependence of the PA signal can provide the thermal imaging of tissue needed for thermal therapeutic approaches. Exogenous contrast agents used for molecular PAI can also be multiplexed to function as drug delivery carriers activated internally or triggered remotely. Therefore, drug delivery and release is an active and expanding area of PAI.

Fundamentally, PAI can be performed in real-time. Real-time imaging is crucial in many diagnostic and therapeutic applications of PAI. In deep-penetrating PAI, array-based ultrasound imaging probes are adopted, thus allowing real-time imaging of tissue where frame rate is primarily limited by the pulse repetition frequency of the laser. Therefore, from an instrumentation perspective, high repetition rate, high pulse energy, single-wavelength, or tunable pulsed laser sources designed for PAI are needed. From a clinical perspective, PAI combined with ultrasound could be easily implemented and adapted by clinicians familiar with ultrasonography. Biomedical PA has seen tremendous growth in the past two decades, yet PA imaging is still in its infancy. Therefore, the wide and rapid advancement of PA, ranging from instrumentation development to regulatory approvals to preclinical and clinical utility, is anticipated in the next decade.

Acknowledgments

Partial support for this work provided by NIH under grants EB008101 and CA149740 is greatly acknowledged. The authors would also like to thank all researchers and scientists who contributed to the field of photoacoustics and, therefore, made this review paper possible.

References

1 Jemal, A. *et al.* (2010) Cancer Statistics, 2010. *CA Cancer J. Clin.* 60, 277–300
2 Fass, L. (2008) Imaging and cancer: a review. *Mol. Oncol.* 2, 115–152
3 Frangioni, J.V. (2008) New technologies for human cancer imaging. *J. Clin. Oncol.* 26, 4012–4021
4 Zhang, H.F. *et al.* (2006) Functional photoacoustic microscopy for high-resolution and noninvasive *in vivo* imaging. *Nat. Biotechnol.* 24, 848–851
5 Siphanto, R.I. *et al.* (2005) Serial noninvasive photoacoustic imaging of neovascularization in tumor angiogenesis. *Opt. Express* 13, 89–95
6 Emelianov, S.Y. *et al.* (2006) Synergy and applications of combined ultrasound, elasticity, and photoacoustic imaging. *IEEE Int. Ultrason. Symp.* DOI: 10.1109/ULTSYM.2006.114
7 Jose, J. *et al.* (2009) Imaging of tumor vasculature using Twente photoacoustic systems. *J. Biophotonics* 2, 701–717
8 Bell, A.G. (1880) Upon the production of sound by radiant energy. *Am. J. Sci.* 20, 305–324
9 Wang, L. (2009) Multiscale photoacoustic microscopy and computed tomography. *Nat. Photonics* 3, 503–509
10 Oraevsky, A. and Karabutov, A. (2003) Optoacoustic tomography. In *Biomedical Photonics Handbook* (Vo-Dinh, T., ed.), pp. 34/31–34/34, CRC Press
11 Xu, M. and Lihong, V.W. (2006) Photoacoustic imaging in biomedicine. *Rev. Sci. Instrum.* 77, 041101
12 Emelianov, S.Y. *et al.* (2009) Photoacoustics for molecular imaging and therapy. *Phys. Today* 62, 34–39
13 Staley, J. *et al.* (2010) Growth of melanoma brain tumors monitored by photoacoustic microscopy. *J. Biomed. Opt.* 15, 40510–40513
14 Oh, J-T. *et al.* (2006) Three-dimensional imaging of skin melanoma *in vivo* by dual-wavelength photoacoustic microscopy. *J. Biomed. Opt.* 11, 034032–034034
15 Manohar, S. *et al.* (2007) Initial results of *in vivo* non-invasive cancer imaging in the human breast using near-infrared photoacoustics. *Opt. Express* 15, 12277–12285
16 Manohar, S. *et al.* (2005) The Twente Photoacoustic Mammoscope: system overview and performance. *Phys. Med. Biol.* 50, 2543
17 Lao, Y. *et al.* (2008) Noninvasive photoacoustic imaging of the developing vasculature during early tumor growth. *Phys. Med. Biol.* 53, 4203
18 Kolkman, R.G.M. *et al.* (2008) Photoacoustic imaging of tumor angiogenesis. In *Photons Plus Ultrasound: Imaging and Sensing 2008: The Ninth Conference on Biomedical Thermoacoustics, Optoacoustics, and Acousto-optics* (Oraevsky, A.A. and Wang, L.V., eds), pp. 685602–685606, SPIE
19 Ku, G. *et al.* (2005) Imaging of tumor angiogenesis in rat brains *in vivo* by photoacoustic tomography. *Appl. Opt.* 44, 770–775
20 Turkbey, B. *et al.* (2009) Imaging of tumor angiogenesis: functional or targeted? *Am. J. Roentgenol.* 193, 304–313
21 Lungu *et al.* (2007) In vivo imaging and characterization of hypoxia-induced neovascularization and tumor invasion. *Int. J. Oncol.* 30, 45–54
22 Li, M. *et al.* (2008) Simultaneous molecular and hypoxia imaging of brain tumors *in vivo* using spectroscopic photoacoustic tomography. *IEEE Int. Ultrason. Symp.* 96, 481–489
23 Höckel, M. and Vaupel, P. (2001) Tumor hypoxia: definitions and current clinical, biologic, and molecular aspects. *J. Natl. Cancer Inst.* 93, 266–276
24 Zharov, V.P. *et al.* (2006) *In vivo* photoacoustic flow cytometry for monitoring of circulating single cancer cells and contrast agents. *Opt. Lett.* 31, 3623–3625
25 Galanzha, E. *et al.* (2009) *In vivo*, noninvasive, label-free detection and eradication of circulating metastatic melanoma cells using two-color photoacoustic flow cytometry with a diode laser. *Cancer Res.* 69, 7926–7934
26 Weight, R.M. *et al.* (2006) Photoacoustic detection of metastatic melanoma cells in the human circulatory system. *Opt. Lett.* 31, 2998–3000
27 Stantz, K.M. *et al.* (2010) Molecular imaging of neutropilin-1 receptor using photoacoustic spectroscopy in breast tumors. In *Photons Plus Ultrasound: Imaging and Sensing 2010* (Oraevsky, A.A. and Wang, L.V., eds), SPIE, pp. O1-7
28 Razansky, D. *et al.* (2007) Multispectral photoacoustic imaging of fluorochromes in small animals. *Opt. Lett.* 32, 2891–2893
29 Kim, G. *et al.* (2007) Indocyanine-green-embedded PEBBLEs as a contrast agent for photoacoustic imaging. *J. Biomed. Opt.* 12, 044020
30 Kim, C. *et al.* (2010) *In vivo* molecular photoacoustic tomography of melanomas targeted by bioconjugated gold nanocages. *ACS Nano* 4, 4559–4564
31 Kim, C. *et al.* (2010) In vivo photoacoustic tomography of chemicals: high-resolution functional and molecular optical imaging at new depths. *Chem. Rev.* 110, 2756–2782
32 Li, P. *et al.* (2008) *In vivo* photoacoustic molecular imaging with simultaneous multiple selective targeting using antibody-conjugated gold nanorods. *Opt. Express* 16, 18605–18615
33 Agarwal, A. *et al.* (2007) Targeted gold nanorod contrast agent for prostate cancer detection by photoacoustic imaging. *J. Appl. Phys.* 102, 064701–064704

34 Li, M. *et al.* (2009) *In-vivo* photoacoustic microscopy of nanoshell extravasation from solid tumor vasculature. *J. Biomed. Opt.* 14, 105071–105073
35 Mallidi, S. *et al.* (2007) Molecular specific optoacoustic imaging with plasmonic nanoparticles. *Opt. Express* 15, 6583–6588
36 Zhang, Q. *et al.* (2009) Gold nanoparticles as a contrast agent for *in-vivo* tumor imaging with photoacoustic tomography. *Nanotechnology* 20, 395102
37 Pan, D. *et al.* (2009) Molecular photoacoustic tomography with colloidal nanobeacons. *Angew. Chem.* 121, 4234–4237
38 Lewinski, N. *et al.* (2008) Cytotoxicity of nanoparticles. *Small* 4, 26–49
39 Shashkov, E. *et al.* (2008) Quantum dots as multimodal photoacoustic and photothermal contrast agents. *Nano Lett.* 8, 3953–3958
40 Mallidi, S. *et al.* (2009) Multiwavelength photoacoustic imaging and plasmon resonance coupling of gold nanoparticles for selective detection of cancer. *Nano Lett.* 9, 2825–2831
41 Yoon, S.J. *et al.* (2010) Utility of biodegradable plasmonic nanoclusters in photoacoustic imaging. *Opt. Lett.* 35, 3751–3753
42 Tam, J.M. *et al.* (2010) Controlled assembly of biodegradable plasmonic nanoclusters for near-infrared imaging and therapeutic applications. *ACS Nano* 4, 2178–2184
43 Levi, J. *et al.* (2010) Design, synthesis, and imaging of an activatable photoacoustic probe. *J. Am. Chem. Soc.* 132, 11264–11269
44 Kim, C. *et al.* (2010) Multifunctional microbubbles and nanobubbles for photoacoustic and ultrasound imaging. *J. Biomed. Opt.* 15, 010510
45 Wilson, K. *et al.* (2010) Photoacoustic and ultrasound imaging contrast enhancement using a dual contrast agent. In *Photons Plus Ultrasound: Imaging and Sensing* (Oraevsky, A.A. and Wang, L.V., eds), pp. M1-5, SPIE.
46 Bouchard, L.S. *et al.* (2009) Picomolar sensitivity MRI and photoacoustic imaging of cobalt nanoparticles. *Proc. Natl. Acad. Sci. U.S.A.* 106, 4085–4089
47 Kim, C. *et al.* (2009) Deeply penetrating *in vivo* photoacoustic imaging using a clinical ultrasound array system. *Biomed. Opt. Express* 1, 278–284
48 Kolkman, R. *et al.* (2008) Real-time *in vivo* photoacoustic and ultrasound imaging. *J. Biomed. Opt.* 13, 050510
49 Niederhauser, J.J. *et al.* (2005) Combined ultrasound and optoacoustic system for real-time high-contrast vascular imaging *in vivo*. *IEEE Trans. Med. Imaging* 24, 436–440
50 Zemp, R.J. *et al.* (2007) Photoacoustic imaging of the microvasculature with a high-frequency ultrasound array transducer. *J. Biomed. Opt.* 12, 010501–010503
51 Zhang, E.Z. *et al.* (2010) Multimodal simultaneous photoacoustic tomography, optical resolution microscopy, and OCT system. In *Photons Plus Ultrasound: Imaging and Sensing* (Oraevsky, A.A. and Wang, L.V., eds), pp. 75640–75647, SPIE
52 Li, L. *et al.* (2009) Three-dimensional combined photoacoustic and optical coherence microscopy for *in vivo* microcirculation studies. *Opt. Express* 17, 16450–16455
53 Zhi, H. *et al.* (2007) Comparison of ultrasound elastography, mammography, and sonography in the diagnosis of solid breast lesions. *J. Ultrasound Med.* 26, 807–815
54 Min, Q. *et al.* (2009) Combined photoacoustic and magneto-acoustic imaging. *IEEE Eng. Med. Biol. Soc.* 4763–4766
55 Mehrmohammadi, M. *et al.* (2010) Pulsed magnetomotive ultrasound imaging using ultrasmall magnetic nanoprobes. *Mol. Imaging* 22, 1–11
56 Xiang, L. *et al.* (2007) Real-time optoacoustic monitoring of vascular damage during photodynamic therapy treatment of tumor. *J. Biomed. Opt.* 12, 014001
57 Kim, J. *et al.* (2009) Golden carbon nanotubes as multimodal photoacoustic and photothermal high-contrast molecular agents. *Nat. Nanotechnol.* 4, 688–694
58 Cui, H. and Yang, X. (2010) *In vivo* imaging and treatment of solid tumor using integrated photoacoustic imaging and high intensity focused ultrasound system. *Med. Phys.* 37, 4777–4781
59 Homan, K. *et al.* (2010) Silver nanosystems for photoacoustic imaging and image-guided therapy. *J. Biomed. Opt.* 15, 021316
60 You, J. *et al.* (2010) Near-infrared light triggers release of Paclitaxel from biodegradable microspheres: photothermal effect and enhanced antitumor activity. *Small* 6, 1022–1031
61 Spirou, G.M. *et al.* (2004) Development and testing of an optoacoustic imaging system for monitoring and guiding prostate cancer therapies. In *Photons Plus Ultrasound: Imaging and Sensing* (Oraevsky, A.A. and Wang, L.V., eds), pp. 44–56, SPIE
62 Larin, K. *et al.* (2005) Monitoring of tissue coagulation during thermotherapy using optoacoustic technique. *J. Phys. D: Appl. Phys.* 38, 2645
63 Shah, J. *et al.* (2008) Photoacoustic imaging and temperature measurement for photothermal cancer therapy. *J. Biomed. Opt.* 13, 034024
64 Su, J. *et al.* (2010) Photoacoustic imaging of clinical metal needles in tissue. *J. Biomed. Opt.* 15, 021306–021309
65 Oraevsky, A.A. *et al.* (1997) Measurement of tissue optical properties by time-resolved detection of laser-induced transient stress. *Appl. Opt.* 36, 402–415
66 Oraevsky, A.A. *et al.* (1995) Lateral and z-axial resolution in laser optoacoustic imaging with ultrasonic transducers. *Proc. SPIE* 2389, 198–208
67 Esenaliev, R.O. *et al.* (1999) Sensitivity of laser opto-acoustic imaging in detection of small deeply embedded tumors. *IEEE J. Selected Top. Quantum Electron.* 5, 981–988
68 Ku, G. and Wang, L.V. (2005) Deeply penetrating photoacoustic tomography in biological tissues enhanced with an optical contrast agent. *Opt. Lett.* 30, 507–509
69 American National Standards Institute (2000) *American National Standard for the Safe Use of Lasers: ANSI Z136. 1-2000*, American National Standards Institute
70 Maslov, K. *et al.* (2008) Optical-resolution photoacoustic microscopy for *in vivo* imaging of single capillaries. *Opt. Lett.* 33, 929–931
71 Mallidi, S. *et al.* (2006) Functional and morphological ultrasonic biomicroscopy for tissue engineers. *Medical Imaging 2006: Ultrasonic Imaging and Signal Processing* (Emelianov, S. and William F. Walker, W.F., eds), pp. 61470Y-1-61470Y-7, Proceedings of the SPIE
72 De la Zerda, A. *et al.* (2010) Ultrahigh sensitivity carbon nanotube agents for photoacoustic molecular imaging in living mice. *Nano Lett.* 10, 2168–2172
73 Homan, K. *et al.* (2010) Prospects of molecular photoacoustic imaging at 1064 nm wavelength. *Opt. Lett.* 35, 2663–2665
74 Xiang, L. *et al.* (2009) Photoacoustic molecular imaging with antibody-functionalized single-walled carbon nanotubes for early diagnosis of tumor. *J. Biomed. Opt.* 14, 021008
75 De La Zerda, A. *et al.* (2008) Carbon nanotubes as photoacoustic molecular imaging agents in living mice. *Nat. Nanotechnol.* 3, 557–562
76 Kim, S. *et al.* Ultrasound and photoacoustic image-guided photothermal therapy using silica-coated gold nanorods: *in-vivo* study. *Proceedings of the 2010 IEEE Ultrasonics Symposium.*(in press).
77 Wang, L. *et al.* (2006) Combined photoacoustic and molecular fluorescence imaging *in vivo*. *IEEE Eng. Med. Biol. Soc.* 190–192
78 Mallidi, S. *et al.* (2009) Ultrasound-based imaging of nanoparticles: from molecular and cellular imaging to therapy guidance. *IEEE International Ultrasonics Symposium* DOI:10.1109/ULTSYM.2009.5441484